Paleoceanography and Paleoclimatology

RESEARCH ARTICLE
10.1029/2019PA003663

Dating Deep-Sea Sediments With ^{230}Th Excess Using a Constant Rate of Supply Model

W. Geibert[1], I. Stimac[1], M. M. Rutgers van der Loeff[1], and G. Kuhn[2]

[1]Marine Geochemistry department, Alfred-Wegener-Institut Helmholtz-Zentrum für Polar-und Meeresforschung, Bremerhaven, Germany, [2]Marine Geology department, Alfred-Wegener-Institut Helmholtz-Zentrum für Polar-und Meeresforschung, Bremerhaven, Germany

Key Points:
- The excess of thorium-230 can be used to date deep-sea sediments in analogy to lead-210
- In an example from the Indian Sector of the Southern Ocean, 230Th CRS-dates agree very well with expected glacial-interglacial cycles
- The dating method, which also yields vertical mass fluxes, works best in an age range of 50,000–450,000 years, depending on local conditions

Supporting Information:
- Supporting Information S1

Correspondence to:
W. Geibert,
walter.geibert@awi.de

Citation:
Geibert, W., Stimac, I., Rutgers van der Loeff, M. M., & Kuhn, G. (2019). Dating Deep-Sea Sediments With ^{230}Th Excess Using a Constant Rate of Supply Model. *Paleoceanography and Paleoclimatology*, *34*. https://doi.org/10.1029/2019PA003663

Received 18 MAY 2019
Accepted 16 OCT 2019
Accepted article online 28 OCT 2019

Corrected 18 DEC 2019
This article was corrected on 18 DEC 2019. See the end of the full text for details.

Abstract We present a dating method for deep-sea sediments that uses the natural radionuclide ^{230}Th (half-life 75,380 years) in analogy to ^{210}Pb with the constant rate of supply (CRS) model. Using an example from the western Indian sector of the Southern Ocean, we demonstrate how sets of values of ^{230}Th, ^{232}Th, and U isotopes activities can supply absolute age information for the last ~450,000 years, given a sufficient precision, resolution, and depth coverage of the analytical data in a suitable core. An assessment of age uncertainties resulting from analytical errors using a Monte Carlo approach and an analytical solution for error propagation shows good agreement. We also investigate errors due to a violation of model assumptions by variable focusing of deep-sea sediments by means of a simulated core. Finally, we use real examples from independently dated sediment cores containing carbonate, using previously existing ^{230}Th data, to test the approach. The consideration of the systematic errors and the examples suggests that the uncertainties are smallest in the central part of the record and that the variability of focusing conditions controls the accuracy of the ^{230}Th CRS dates. Our own example demonstrates an excellent agreement of the ^{230}Th CRS method with independent age constraints, adding an important tool for dating marine records that does not depend on the presence of carbonate. The obtained values are also suitable to calculate ^{230}Th-normalized preserved vertical rain rates of various sedimentary compounds, permitting an improved quantitative comparison of marine paleorecords with other archives like ice cores.

Plain Language Summary This study explores a new way of determining the age of sediments at the seafloor. It exploits the fact that a rare variety of the element thorium (^{230}Th) that occurs naturally in the ocean is supplied to the seafloor at a constant rate. Due to its natural radioactivity with a half-life of 75,380 years, it can be used to determine the age of sediments back to approximately 450,000 years. The mathematical approach is very similar to a well-established method for ^{210}Pb (22-year half-life) that reaches back about 100–150 years. In this study, we present this method based on an example from the Southern Ocean, introducing the measurement techniques used, the calculations, and the results and discussing the agreement with alternative methods. The importance of the method lies in the fact that it can be used to date a very abundant type of seafloor sediments that do not contain carbonate microfossils and that therefore cannot be dated or only with a larger uncertainty.

1. Introduction

Determining the age of deposition of deep-sea sediments can be a difficult undertaking. Most approaches to date such sediments rely on microfossils, which are not always present. If carbonaceous microfossils are present in sufficient amounts, radiocarbon dating can be applied back to about 50 kiloyears (Reimer et al., 2016). Oxygen isotopes in such carbonaceous microfossils can be used to match individual marine records to the global oxygen isotope stack (Lisiecki & Raymo, 2005), reaching back millions of years. In a biostratigraphic approach, identifying the first or last occurrence of characteristic species can also provide firm age constraints. However, if microfossils are absent, most common dating approaches fail. Where present, ash layers or other characteristic deposits can still be used to infer absolute age information. Still, in large parts of the ocean, none of the approaches above can be used, due to the absence of sufficiently preserved carbonate, suitable microfossils in general, and the absence of other layers of known deposition time.

The longer-lived naturally occurring radionuclides of the uranium and thorium series ^{230}Th, ^{231}Pa, and ^{234}U were early candidates to address this problem on glacial-interglacial timescales (Goldberg & Koide, 1962;

Ku, 1965; Ku & Broecker, 1965). On shorter timescales up to ~150 years—as often given for continental records like lacustrine sediments or peat bogs—^{210}Pb supplied from the atmosphere by decay of ^{222}Rn has become an indispensable tool for deriving age information (Appleby, 1998). However, due to the low sedimentation rates in the range of mm to cm/ky for pelagic marine environments, the unsupported fraction of this relatively short-lived radionuclide ^{210}Pb (22.3-year half-life) remains at the very surface of the sediment, unless its signal is mixed within the bioturbated layer. This layer is often 5–15 cm deep, rendering ^{210}Pb almost useless for dating in low sedimentation rate environments. The radionuclides ^{230}Th (half-life 75,380 years), ^{231}Pa (half-life 32,760 years), and ^{234}U (half-life 245,500 years) that live beyond the bioturbated layer are still the most promising candidates for dating Quaternary deposits. U is mobile in sediment pore waters, which results in large uncertainties when dating this open system via ^{234}U (Ku, 1965). This leaves the strongly particle-bound radioisotopes ^{230}Th and ^{231}Pa, which both share uranium in seawater as the well-defined source, as the best candidates. In fact, their flux from the water column, though locally variable to some extent (Henderson et al., 1999; van Hulten et al., 2018), is very well constrained, often better than the much more variable atmospheric ^{210}Pb$_{ex}$ flux. For pelagic "red clay" sediments, these radionuclides are the key tool that have informed us about the sedimentation rates of deep-sea sediment in the absence of carbonates (Goldberg and Koide (1962), for a recent example see Volz et al. (2018)). However, previous approaches to use these longer-lived isotopes for dating were based on either assuming a constant initial concentration or a constant initial production ratio for Pa/Th, both of which are not necessarily found in marine sediments.

The amount of ^{230}Th and ^{231}Pa present in deep-sea sediments has been found to sometimes differ considerably from the known production in the overlying water column. This has been in part attributed to sediment redistribution (focusing/winnowing, see Thomson et al. (1993) or François et al. (2004)) and partly to advection or boundary scavenging in the ocean (Anderson et al., 1983), which leads to deviations between the expected production rate and the underlying sedimentary inventory (Yang et al., 1986). Here, we focus on the nuclide ^{230}Th, which is less affected by lateral transport than ^{231}Pa.

The activity of ^{230}Th found in a certain depth of sediment depends on a number of variables. It depends on salinity and depth of the overlying water column because the uranium concentration in seawater is proportional to salinity; on the direct or indirect effects of boundary scavenging; on dilution by variable particle flux, on production within the sediment by lithogenic and authigenic ^{234}U, and eventually on the age of the sediment via decay, which will be the dominating effect on ^{230}Th activity after a couple of half-lives. As most of these variables can be constrained once age is known, leaving dilution by particle flux as the main unknown, ^{230}Th in marine sediments has been an essential tool for reconstructing past particle fluxes and determining focusing factors (François et al., 2004; Frank et al., 1995).

Here, we take the opposite approach. The question that we address here is whether the excess of ^{230}Th (^{230}Th$_{ex}$) supplied to deep-sea sediments from the overlying water column can also be used to date deep-sea sediments, much in analogy to the shorter-lived ^{210}Pb, using the constant rate of supply (CRS) model by Appleby and Oldfield (1978) and Appleby et al. (1979). The particular merit of this model with respect to ^{230}Th is that it calculates the age based on the complete radionuclide inventories above and below the respective depth of interest. Therefore, it does not respond to changes in vertical particle flux that dilute the signal, which are known to occur for ^{230}Th. Even lateral input by the effects of focusing/winnowing or the combined effects of advection and scavenging should be irrelevant, as long as they are on average the same above and below the depth of interest. In analogy to ^{210}Pb$_{ex}$ CRS dates, the method requires an assessment of the complete ^{230}Th$_{ex}$ inventory, which means measuring in sufficient resolution to a depth where all unsupported ^{230}Th has decayed. Only with the advent of mass spectrometric measurements of ^{230}Th, this has become a realistic undertaking on a larger scale, delivering the required resolution and the required precision. To our knowledge, the principle of this approach for ^{230}Th has only once been applied to marine sediments by Kominz et al. (1979), integrating over full glacial-interglacial cycles, later on transferred to manganese nodules by Bollhöfer et al. (1999).

We demonstrate the application of this method using sediment core PS63/146-2 (Fütterer & Kattner, 2005) from the Indian sector of the Southern Ocean just south of the southwest Indian Ridge. This sediment core consists of diatom muds to diatom oozes with a mean of 54% and a range of 21%–99% biogenic opal content and <1% carbonate. We first introduce our analytical techniques before we test the suitability of the CRS model with ^{230}Th$_{ex}$ as a new dating tool for deep-sea sediments that does not require carbonate

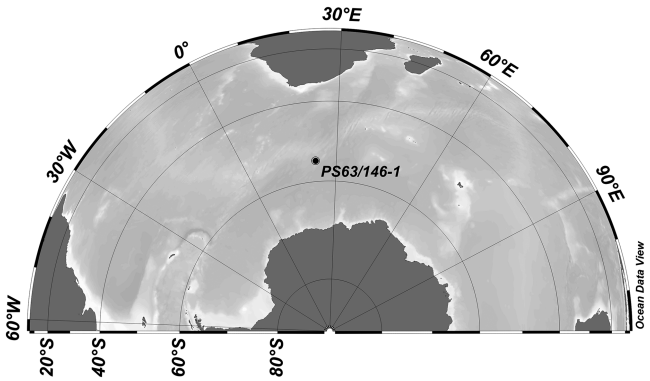

Figure 1. Map of the Atlantic and Indian sector of the Southern Ocean, centered on gravity core PS63/146-2.

preservation or microfossils. Our approach follows largely François et al. (2004) for determining the contributions to the combined ^{230}Th signal in order to extract the signal of $^{230}Th_{ex}$. We then combine this information with the CRS model of Appleby and Oldfield (1978) and discuss how we can use the obtained information to learn about sedimentation rates, and we compare the obtained dated record to known dates of marine glacial-interglacial patterns. We then demonstrate how the obtained dates can be combined with other information from U/Th series isotopes and elemental analyses to reconstruct past biogeochemical fluxes in pelagic settings.

2. Materials and Methods

2.1. Sediment Core PS63/146-2

Gravity core PS63/146-2 (see Figure 1) was taken during Polarstern cruise ANT XX/2 (Fütterer & Kattner, 2005) in the western Indian sector of the Southern Ocean, right at the northeastern and eastern boundary of the Weddell Gyre (55.32°S, 23°E, 4800-m water depth). This region is currently highly productive, featuring some of the highest opal fluxes in surface sediments of the open Southern Ocean (Geibert et al., 2010).

2.1.1. Physical Properties

In order to date a sediment core with the $^{230}Th_{ex}$ CRS approach, we need to know the contribution of each depth interval to the $^{230}Th_{ex}$ inventory. We can determine the inventory of $^{230}Th_{ex}$ [dpm/cm^2] for a given depth interval L as the product of the activity A of $^{230}Th_{ex}$ [dpm/g] (measured on dried homogenized sediment), the water-free density WFD [g/cm^3] of the sediment, and L [cm]:

$$I_i = A*WFD*L \tag{1}$$

The WFD closely resembles the dry bulk density DBD, but it includes the contribution of dried salt from pore water. WFD was calculated from wet bulk density modified after Niessen et al. (2013) and Kuhn et al. (2017) and a specific porosity, with salt assumed to be in a solid phase (φ_s; volume %):

$$WFD = WBD - \frac{\varphi_s}{100} \tag{2}$$

$$WBD = \frac{100}{\frac{100-w}{\rho_d} - \frac{w*r}{\rho_s} + \frac{w*100}{96.5*\rho_w}} \tag{3}$$

$$\varphi_s = \frac{100*w}{\frac{100-w}{\rho_d} - \frac{w*r}{\rho_s} + w} \tag{4}$$

Wet bulk density was calculated from measurements of water content (*w, weight %*) and density of the milled dry sediment (ρ_d; micromeritics gas-pycnometer AccuPyk 1330); ρ_s is density of salt (2.1 g/cm^3), and *r* is the mass ratio of salt to water (= 0.036, at 3.5% salinity). For pore water density (ρ_w), we assumed a constant of 1.03 g/cm^3 because pore water density for in situ conditions differ insignificantly (0.99–1.055 g/cm^3) (Kuhn et al., 2017). As an alternative to the calculation-based approach above, one could simply determine the dry weight of a known sediment volume to determine the WFD.

The reason for using WFD instead of DBD here is that in contrast to most terrestrial settings, marine pore waters contain salt that contributes to the mass of a dried sample. Therefore the DBD (g/cm^3) of marine sediments, which is supposed to be salt-corrected, is not exactly the right parameter when converting measured activities of the salt-containing samples to a sediment volume. However, when deriving vertical mass fluxes later on, the contribution of salt has to be subtracted, and we have to use the usual (salt-corrected) DBD value

(φ = porosity as volume %):

$$DBD = WBD - \frac{\varphi}{100} \quad (5)$$

$$\varphi = \frac{100 * \frac{w*100}{96.5*\rho_w}}{\frac{100-w}{\rho_d} - \frac{w*r}{\rho_s} + \frac{w*100}{96.5*\rho_w}} \quad (6)$$

When calculating the normalized fluxes of individual components, the salt correction can be ignored if both ^{230}Th and the component of interest have been measured in the salt-containing matrix, resulting in identical dilution.

Once WFD is known, using equation (1), we will obtain a ^{230}Th inventory I_i in (dpm/cm^2) for this interval. The length of the interval *i* can either have been sampled completely, yielding an average ^{230}Th activity, or samples have been taken at smaller intervals. In the latter case, we assume a constant activity of ^{230}Th for all depths for which we have no other closer measurement. For example, if we have samples at 10–11, 20–21, and 30–31 cm, then we would expect the value from 20–21 cm to represent the depth from 15.5–25.5 cm. L would be 10 cm in this case.

2.2. (Radio)Chemical Analyses

2.2.1. Sediment Full Digestion

In order to determine ^{230}Th, ^{232}Th, ^{238}U, and ^{234}U together with a number of bulk element concentrations, about 75 mg of freeze-dried and ground marine sediment, homogenized from several g, was digested in a pressure-assisted microwave digestion system (CEM MarsXpress), using a Mars XpressVap evaporation accessory. Samples were digested and analyzed in batches of 24, each consisting of 2 procedural blanks, 2 reference material samples for U-series isotopes (UREM-11, Hansen, and Ring), and 2 reference material samples for elemental concentrations (NIST2702 or NRC MESS-4), together with 18 samples of unknown composition. The sediments and reference materials were weighed into the fluoropolymer (TFM) digestion vessels together with a known amount of ^{229}Th (11 pg) and ^{236}U (770 pg) for isotope dilution analysis. Added to the samples were 0.5-mL HF Suprapur®, 2-mL concentrated HNO_3, and 3-mL concentrated HCl (the latter two were single distilled in a quartz sub-boiling still), and the mixture was exposed under pressure to temperatures of at least 230°C for 30 minutes. The liquid in the samples was then evaporated using the XpressVap accessory. In a second digestion step, 5 mL of 1-M HNO_3 were added to each sample, which were then exposed to temperatures of at least 200°C in the microwave system. The samples were quantitatively transferred to centrifuge vials, filled to 25 mL, their weight noted for gravimetric calculation of the dilution factor, and a known mass of about 5 mL for a 20% subsample of the digested material was taken from each sample for multielement analyses via inductively coupled plasma optical emission spectroscopy and sector field inductively coupled plasma mass spectrometry (results not shown here). The remainder of the samples (80%) was used for the determination of Th and U isotopes after a purification and separation via ion exchange chromatography. The sample-processing scheme following the full digestion of samples, including a list of analyzed elements, is shown in Figure 2.

2.2.2. Purification of Th and U Fractions

For the removal of most of the matrix elements in the Th-U fraction of the samples, a small amount of purified iron chloride solution was added (50 µL of a purified 50 g/L $FeCl_3$-solution in HCl). This iron was precipitated, together with any natural iron present, by adding ammonia until a pH of 8.5–9 was reached, following an established protocol of Anderson and Fleer (1982). The precipitate containing Th and U was separated from the supernatant by centrifugation, redissolved with nitric acid, and reprecipitated. These steps were repeated twice. Eventually, the precipitate was washed with ultrapure water, centrifuged again, the supernatant discarded, and dissolved for in final volume of ca. 2 mL 3-M nitric acid. After adding 150 µL of 1-M Al $(NO_3)_3$-solution, the sample solution was added to ion exchange columns containing approximately 2-mL UTEVA resin, preconditioned with 3-M HNO_3. Iron and most other remaining elements were eluted with three column volumes (CV) of 3-M HNO_3. Then thorium was eluted and collected separately with one CV of 9-M HCl followed by two CV 5-M HCl. Eventually, the uranium fraction was eluted with three CV 0.02-M HCl and collected separately. The thorium and uranium fractions were evaporated to near dryness and redissolved in ~5 mL 1-M nitric acid for analysis.

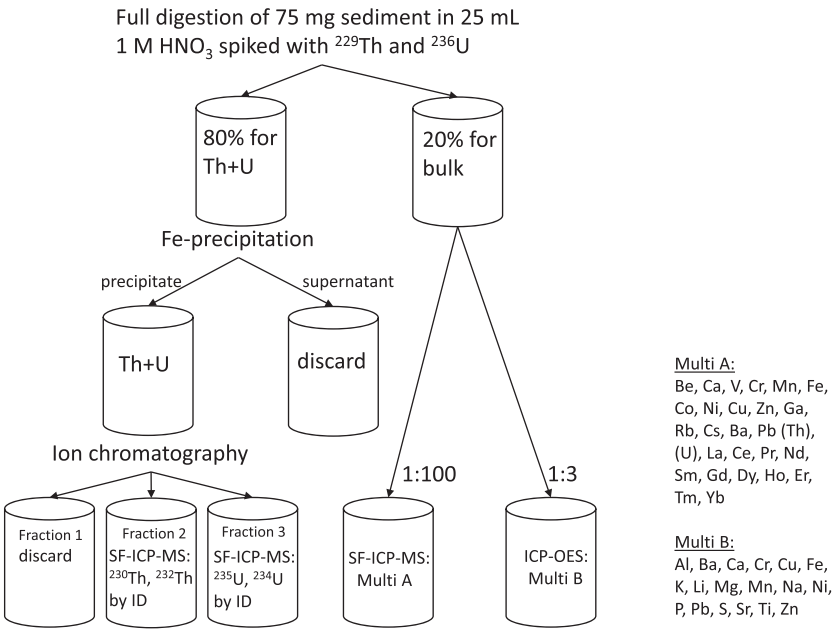

Figure 2. Sample-processing scheme following the sediment full digestion as described in the text. The results for elemental concentrations are not shown here as they are not required for the dating approach, but we mention them to give a complete impression of the analytical procedure. SF-ICP-MS = Sector field inductively coupled plasma mass spectrometry; ID = Isotope dilution; ICP-OES = Inductively coupled plasma optical emission spectroscopy. Multi = Multielement analysis with external calibration, using an internal standard.

2.2.3. Isotope Dilution Analysis of U-Series Isotopes

The U-series isotopes were analyzed on an Element2 sector field inductively coupled plasma mass spectrometry. Uranium isotopes were analyzed in low resolution (R = 300), using a cyclonic spray chamber. Mass bias was monitored with a uranium solution of known natural isotopic composition, using the masses 238 and 235. Due to the high intensities for ^{238}U in our natural samples, the ^{238}U peak was avoided here, and instead, ^{235}U was measured together with ^{234}U and the artificial tracer ^{236}U. ^{238}U concentrations and subsequently activities were calculated from ^{235}U assuming an atom ratio of 137.88.

Thorium was analyzed using an Apex IR desolvation device for increasing sensitivity. The Element2 mass spectrometer was operated here in a special resolution of R = 2000 for thorium analyses. This resolution results in flat peak tops like typically obtained for low resolution measurements but yielding a better abundance sensitivity, thus allowing a reduction of the low mass tailing of ^{232}Th on ^{230}Th. This tailing from mass 232 was monitored and corrected for by measuring at masses 231.5 and 230.5, together with ^{230}Th as the main target and ^{229}Th as an artificial tracer. The sensitivity in this resolution is reduced by about a factor of seven compared to low resolution, but the lower tailing correction results in better accuracy and precision for low ^{230}Th/^{232}Th ratios. This is not a requirement for the method presented here, but it extends its range due to the overall reduced uncertainties for older parts of the record. External precision was monitored here using the reference material MESS-4 (not certified for ^{230}Th), which was later on measured against certified reference material Irish Sea sediment IAEA-385 (Pham et al., 2008). For the record presented here, ^{230}Th in MESS-4 was found to be 2.925 ± 0.097 dpm/g (3.3%, n = 10). For the later measurement against IAEA-385, MESS-4 was measured at 2.824 ± 0.044 dpm/g (1.56%, n = 16) versus IAEA-385 with 1.858 ± 0.0297 dpm/g (1.60%, n = 16). The certified value of ^{230}Th in IAEA-385 is 1.89 ± 0.108 dpm/g ^{230}Th.

2.2.4. Analysis of a Large Set of Elements on the Same Full Digestion

While we do not discuss the full elemental composition of the presented example, we show the complete scheme of the analytical procedure here in Figure 2 in order to give an explanation for the amounts analyzed and to show the potential of the method for calculating elemental fluxes.

3. Data and Evaluation Methods

The following section describes the handling of the data and the sequential calculations that lead to CRS dates, various proxy records, fluxes of sedimentary compounds, and an assessment of data quality. A flowchart aiding with orientation in the calculation process is provided in the supplementary material.

3.1. Stepwise Determination of $^{230}Th_{ex}$ and Dating

3.1.1. The Components of ^{230}Th in Marine Sediments

^{230}Th in deep-sea sediments is contributed by three sources. The first source is the flux from the overlying water column, which is the component that we need to know for our dating approach. This component (excess ^{230}Th, $^{230}Th_{ex}$) exceeds ^{230}Th in equilibrium with its parent ^{234}U in the sediment ("supported"):

$$^{230}Th_{total} = \overbrace{^{230}Th_{ex} + \underbrace{^{230}Th_{auth} + {}^{230}Th_{lith}}_{^{230}Th_{supp}}}^{^{230}Th_{nolith}} \quad (7)$$

The remainder of ^{230}Th in marine sediments, supported ^{230}Th ($^{230}Th_{supp}$; see equation (7)), can in turn have two sources. It consists of a lithogenic fraction ($^{230}Th_{lith}$), which is invariably present and a contribution from authigenic uranium (labeled here as $^{230}Th_{auth}$), which may accumulate in sediments as dissolved uranium from the bottom waters diffuses into sediments when oxygen concentrations are low and which plays a larger role for older sediments due to the slow ingrowth of ^{230}Th from ^{234}U. The importance of these fractions varies considerably between settings: In shallow, high flux environments, initial $^{230}Th_{ex}$ activities can be below 5 dpm/g, and corrections for lithogenic or authigenic contributions can be large. In deep, low flux environments that can reach ^{230}Th activities of >100 dpm/g, the relative contribution of supported ^{230}Th is relevant only in the oldest part of the core, and authigenic U may be absent altogether, extending the dating range of ^{230}Th.

All of the ^{230}Th components introduced above may change over time. $^{230}Th_{ex}$ simply follows radioactive decay, because it is only supplied from above, and supply stops when it is buried below the sediment surface. $^{230}Th_{lith}$ may be assumed to be invariant over time, with a small exception for sediment particles arriving at the sediment surface slightly depleted in ^{234}U due to a recoil effect and not yet in complete equilibrium with ^{230}Th and for the usually small variations in lithogenic U content. $^{230}Th_{auth}$ is growing over time, as authigenic ^{234}U that decays to ^{230}Th is incorporated into the sediment after deposition, and ^{230}Th then grows into a transient equilibrium with this component, following its own half-life of 75,380 years. Because we can only measure total ^{230}Th, we need to determine $^{230}Th_{lith}$ and $^{230}Th_{auth}$ (if present) indirectly in order to calculate $^{230}Th_{ex}$. In the following section, we use data from the gravity core PS63/146-2 to demonstrate the sequential correction of the ^{230}Th signal to obtain $^{230}Th_{ex}$ for a dating approach. We would like to point to the considerations provided by Bourne et al. (2012), which we did not use here but which contain a detailed assessment of the individual contributions and which are also well suited for deriving corrected $^{230}Th_{ex}$ values. The full data set is supplied in the supplementary data and available via the Pangaea data base.

3.1.2. Determining the Lithogenic Component of ^{230}Th

Equation (7) implies that in order to calculate $^{230}Th_{ex}$ from our measured value $^{230}Th_{total}$, we need to know $^{230}Th_{supp}$, which is the sum of $^{230}Th_{lith}$ and $^{230}Th_{auth}$. Here, we follow sequence of corrections that uses first a correction of ^{230}Th for $^{230}Th_{lith}$ only. This will be used to calculate a preliminary age, which can later be used to approximate $^{230}Th_{auth}$.

Various approaches have been chosen in the past to correct ^{230}Th for lithogenic ^{230}Th, depending on the setting and the application. The most straightforward way to correct lithogenic ^{230}Th (assumed here to be in equilibrium with ^{234}U for simplicity) is to infer the lithogenic fraction of its parent ^{234}U from an element or isotope of strictly lithogenic origin like Al, Ti, or ^{232}Th, using a generic U/element ratio for the lithogenic fraction. The common thorium isotope ^{232}Th, representing >99.99% of the elemental concentration of thorium, is the preferred choice here because it is usually measured as part of the ^{230}Th measurement. Typically, the concentration of ^{232}Th is 10.7 ppm (2.6 dpm/g) in the lithogenic fraction of deep-sea sediments (McGee et al., 2007; Taylor & McLennan, 1995). Exceptions do occur near special geological environments, but the

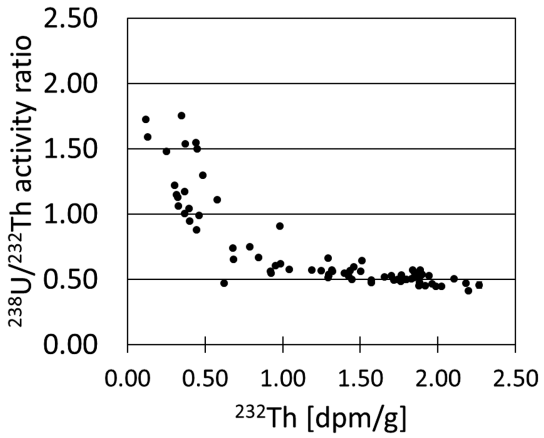

Figure 3. $^{238}U/^{232}Th$ activity ratio of bulk sediment versus the respective ^{232}Th value. High ^{232}Th is indicative of a high lithogenic content. A value of 2.6 dpm/g (10.7 ppm, see text) would represent an exclusively lithogenic endmember. Dilution of ^{232}Th may occur by phases that contain very low ^{238}U and ^{232}Th (like biogenic opal), leaving the $^{238}U/^{232}Th$ largely unchanged. Only authigenic uranium should increase the $^{238}U/^{232}Th$ ratio significantly. This graph therefore reveals the $^{238}U/^{232}Th$ of the lithogenic endmember required in equation (8).

value above has been widely and reliably used. However, ^{232}Th in this step is only used to infer the activity of $^{234}U_{lith}$ via $^{238}U_{lith}$. This can be done once the $^{238}U/^{232}Th$ activity ratio of the lithogenic endmember is known, which is the value that is needed to solve equation (8). We can then infer $^{230}Th_{lith}$ using the following set of equations:

$$^{238}U_{lith} = {}^{232}Th^{*}\left[\frac{^{238}U}{^{232}Th}\right]_{lith} \quad (8)$$

and

$$^{230}Th_{lith} \approx {}^{234}U_{lith} \approx {}^{238}U_{lith} \quad (9)$$

A plot of the total $^{238}U/^{232}Th$ activity ratio (AR) versus ^{232}Th activity for all samples in a core (Figure 3) can be used to reveal the lithogenic $^{238}U/^{232}Th$ activity ratio, if there are at least a few sections without authigenic U in the core. The lowest ratios observed, often around 0.4, will reflect the parts without authigenic U. However, the $^{238}U/^{232}Th$ activity ratio is known to vary between regions and occasionally with time, so 0.4 cannot be used as a universal choice. Here, we used a value of 0.48 as the most appropriate choice for the $^{238}U/^{232}Th$ activity ratio for PS63/146-2 (see Figure 1). Based on this, we can calculate lithogenic ^{238}U according to equation (8).

In the next step, we determine the lithogenic fraction of ^{230}Th ($^{230}Th_{lith}$) and ^{230}Th without the lithogenic component ($^{230}Th_{nolith}$).

The value of $^{238}U_{lith}$ from equation (8) can now be used to determine $^{230}Th_{lith}$ (equation (9)) in a first approximation if we assume the lithogenic $^{234}U/^{238}U$ activity ratio to be unity. Bourne et al. (2012) recommend a value of 0.96 ± 0.04 instead of unity, which may be justified in many settings. Here, this correction was of minor importance, as seen in rather homogeneous $^{234}U/^{238}U$ ratios around unity (Figure 4). We can now also calculate $^{238}U_{auth}$ (also shown in Figure 4) following equation (10):

$$^{238}U_{auth} = {}^{238}U_{total} - {}^{238}U_{lith} \quad (10)$$

In the absence of authigenic U, the subtraction of $^{230}Th_{lith}$ from $^{230}Th_{total}$ ($^{230}Th_{nolith}$) should result in values close to zero for the oldest parts of the sediment core because all remaining ^{230}Th would originate from $^{230}Th_{ex}$, which has decayed. Once we know $^{230}Th_{lith}$, we can calculate ^{230}Th without the lithogenic fraction ($^{230}Th_{nolith}$, see equation (7)), which is already a good approximation for $^{230}Th_{ex}$ in many settings.

Now only $^{230}Th_{auth}$ is missing for a precise knowledge of $^{230}Th_{ex}$. The potential contribution of an authigenic fraction is also a main difference to the CRS model with $^{210}Pb_{ex}$, for which the determination of the supported fraction is more straightforward. $^{230}Th_{auth}$ can be approximated using the following set of equations:

$$^{234}U_{auth} = {}^{238}U_{auth}{}^{*}1.15 \quad (11)$$

$$^{230}Th_{auth} \approx {}^{234}U_{auth}{}^{*}\left(1 - e^{-\lambda_{230Th}{}^{*}t}\right) \quad (12)$$

Equation (12) implies that $^{230}Th_{auth}$, which we need for a precise calculation of $^{230}Th_{ex}$, depends on the time t that it had to grow in from ^{234}U. As the accumulation of U_{auth} occurs near the sediment-water interface, this time t should be not far away from the time of deposition, which we use as an approximation to calculate ingrowth. However, in the absence of a known deposition time, we have to proceed initially without a correction of $^{230}Th_{ex}$ for supported ^{230}Th from authigenic U. We will therefore first calculate a preliminary CRS

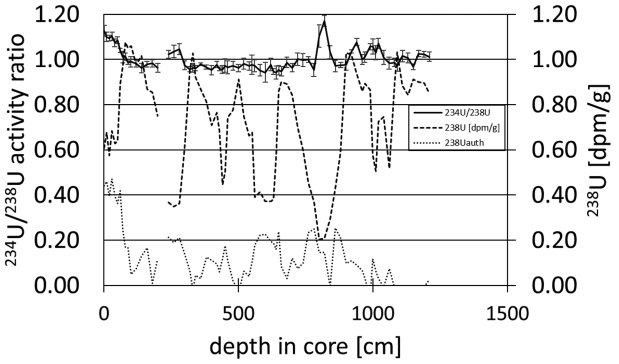

Figure 4. ^{238}U, $^{234}U/^{238}U$ activity ratio and authigenic ^{238}U versus depth core PS62/146-2. With few exceptions, $^{234}U/^{238}U$ is close to unity, and there is only a small contribution of authigenic U in this core.

age with $^{230}Th_{nolith}$, which we then use in a following step to correct $^{230}Th_{auth}$ with which we can calculate $^{230}Th_{ex}$ more accurately, improving the age model in a second iteration.

3.1.3. Preliminary Dating to Derive $^{230}Th_{auth}$

In order to date a sediment core with the $^{230}Th_{ex}$ CRS approach, we need the contribution of each depth interval to the $^{230}Th_{ex}$ inventory. We can determine the inventory of $^{230}Th_{ex}$ (dpm/cm^2) for a given depth interval L as the product of the activity A of $^{230}Th_{ex}$ (dpm/g) (measured on dried homogenized sediment), WFD (g/cm^3) of the sediment, and L (cm), as described above. The sum of the individual inventories is the total inventory of the core (dpm/cm^2).

Our method to calculate a ^{230}Th CRS age follows a method of Appleby and Oldfield (1978), based on an older approach of Goldberg (1963). For each age t of a discrete layer in a sediment core, there is a unique ratio of the entire inventory of a radionuclide in a core to that below this discrete layer. Their equation (9) can be rewritten for $^{230}Th_{ex}$, simply replacing the decay constant of ^{210}Pb with that of ^{230}Th:

$$t = \frac{1}{\lambda_{230Th}} * \ln\left(\frac{I}{I_{\geq i}}\right) \tag{13}$$

With $I_{\geq i}$ being the $^{230}Th_{ex}$ (or $^{230}Th_{nolith}$) inventory beneath depth i in the sediment, I being the complete inventory of $^{230}Th_{ex}$ (or $^{230}Th_{nolith}$), and λ_{230Th} being the decay constant of ^{230}Th, we can calculate the age t. The result of the calculation of age versus sediment depth for our example, using $^{230}Th_{nolith}$ to approximate $^{230}Th_{ex}$ in a first iteration, is shown in Figure 5 (left panel).

3.1.4. Obtaining $^{230}Th_{ex}$ and the Final CRS Ages

With this initial age estimate, we can calculate the contribution of ^{230}Th from U_{auth} for each sample according to equation (7). Small deviations of the first iteration of ages from the actual age will have little effect on the calculated ^{230}Th ingrowth from authigenic U.

Now we can calculate the final value for $^{230}Th_{ex}$ for each sample:

$$^{230}Th_{ex} = {}^{230}Th_{total} - {}^{230}Th_{lith} - {}^{230}Th_{auth} \tag{14}$$

The resulting depth distribution of $^{230}Th_{ex}$ in comparison to $^{230}Th_{total}$ is shown in Figure 6.

With this final value for $^{230}Th_{ex}$ (Figure 6, bottom panel), we recalculate the age as the final age determination (Figure 5, right panel) using equation (13) and equation 1. In our example, the age difference due to $^{230}Th_{auth}$ is up to 7% in the older parts of the record.

3.2. Application of $^{230}Th_{ex}$ and the Age Information to the Chemical Record

3.2.1. Comparing the Total $^{230}Th_{ex}$ Inventory to the Expected Production

Now that we have determined $^{230}Th_{ex}$, we can compare the inventory of $^{230}Th_{ex}$ to that expected from production. Adding up the partial inventories of all sample intervals, our core yields a complete inventory 1743 dpm/cm^2.

The expected flux of ^{230}Th from the water column can be calculated as a function of depth, assuming a salinity of 35 (see also François et al. (2004)):

$$P = \beta * z \tag{15}$$

P being the production of ^{230}Th in the overlying water column in dpm·m^{-2}·yr^{-1},

β being the production rate per volume of seawater of 0.0267 dpm·m^{-3}·yr,

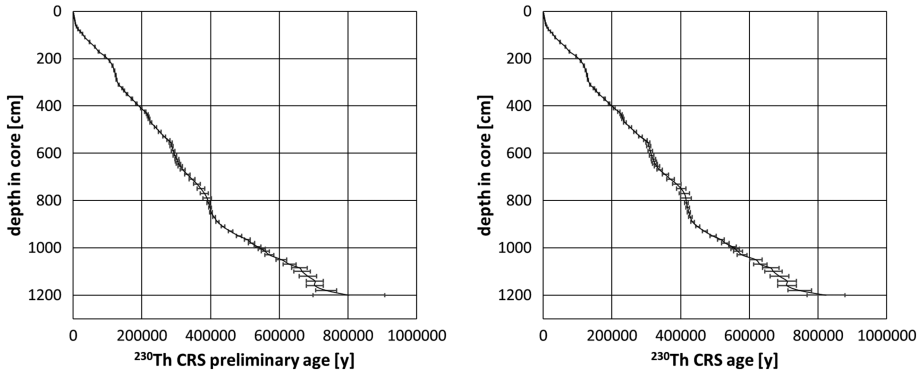

Figure 5. Left: Initial age calculation based on ^{230}Th corrected for lithogenic, but not for authigenic U contributions. This age is used to estimate ingrowth of ^{230}Th from authigenic U and obtain the final age (right panel). Right: Final ^{230}Th CRS age after consideration of ^{230}Th grown in from authigenic uranium. The errors represent one standard deviation, assuming a normal distribution of the Monte Carlo uncertainties (see text).CRS = Constant rate of supply.

and z being the water depth in m.

$$I_{\mathrm{exp}} = \frac{P}{\lambda} \tag{16}$$

The expected production from the overlying water column is 1394 dpm/cm^2, yielding a ratio of expected versus actual inventory of 1.28, which indicates that on average, slight focusing prevails at the core site.

3.2.2. $^{230}Th_{ex}^{0}$ as a Plausibility Control

Using our ^{230}Th CRS ages, we can correct $^{230}Th_{ex}$ for decay and obtain $^{230}Th_{ex}$ at the time of deposition, $^{230}Th_{ex}^{0}$ (Figure 7). At first sight, using ^{230}Th ages to correct ^{230}Th for decay may seem like a circular argument. However, the age calculation is based on all ^{230}Th values above and below a specific depth, whereas the decay correction is only applied to an individual value.

While we cannot a priori expect $^{230}Th_{ex}^{0}$ to be constant through time due to variations with particle flux, a systematic offset of ^{230}Th CRS ages would be expected to be seen as a trend in the data, and it is reasonable to expect that we find similar values for $^{230}Th_{ex}^{0}$ in interglacials and glacials, respectively. The distribution shown in Figure 7 is therefore fully plausible and supports the correctness of the ^{230}Th CRS ages.

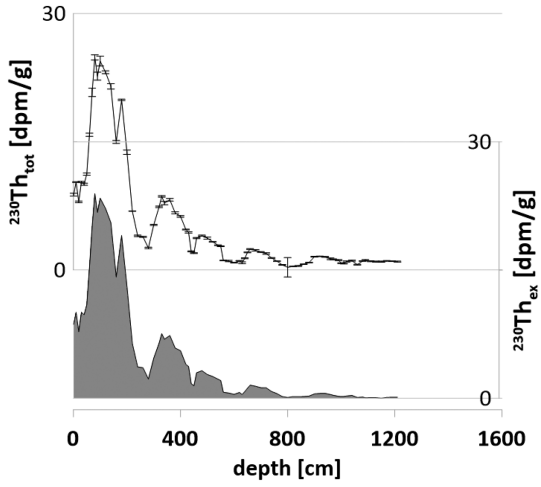

Figure 6. Total ^{230}Th (upper graph) and $^{230}Th_{ex}$ (lower graph) versus depth for core PS63/146-2. The error bars represent one sigma (analytical error including procedural blanks). $^{230}Th_{ex}$ is obtained after subtracting the lithogenic fraction from $^{230}Th_{tot}$, then calculating a preliminary ^{230}Th CRS age, and then also subtracting $^{230}Th_{auth}$.

3.2.3. Calculation of Vertical ^{230}Th-Normalized Fluxes

The knowledge of the activity of $^{230}Th_{ex}^{0}$ allows us to calculate the preserved vertical flux according to (François et al., 2004), including a correction for the mass contributed by salt in the dried samples:

$$^{pr}F_{v} = \frac{P}{^{230}Th_{ex}^{0}} * (1 - f_{s}) \tag{17}$$

The variable $^{pr}F_{v}$ reflects the salt-corrected vertical total mass flux into the sediment. The expression "vertical" indicates that it is implicitly corrected for lateral contributions by focusing, that is, it shows the ^{230}Th-normalized mass flux. The production of ^{230}Th from the overlying water column is written as P, and the mass fraction of salt is written as f_s. Once the salt-corrected mass flux is known, the contributions of individual sediment components can be calculated from their fraction of the total mass f_i:

$$prF_{v}^{i} = prF_{v} * f_{i} \tag{18}$$

As outlined above, the lithogenic fraction f_{lith} of marine sediments can be assumed for most locations to contain a concentration of 10.7 ppm. Thus, we can calculate the lithogenic fraction f_{lith} from the concentration of ^{232}Th in a sample:

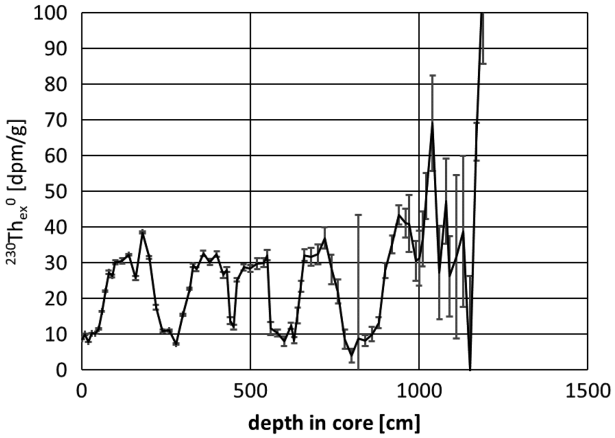

Figure 7. $^{230}Th_{ex}{}^{0}$ (calculated using CRS dates) versus depth. The error (1 s) due to the decay correction increases with depth. In our example, values beyond 900 cm (450,000 years, six ^{230}Th half-lives) obviously become less reliable.

$$f_{lith} = \frac{\left[^{232}Th\right]}{10.7} \tag{19}$$

Here, the concentration of ^{232}Th is assumed to be shown as mass fractions in parts per million (ppm).

The ^{230}Th-normalized lithogenic flux for each sample can then be determined:

$$prF_v^{lith} = prF_v{}^{*}f_{lith} \tag{20}$$

For locations that receive no other lithogenic input but dust, this value will be the dust flux (see Sayles et al. (2001) and Martínez-Garcia et al. (2009)).

The calculation of the flux of biogenic opal can be performed accordingly (taking into consideration if the fraction of biogenic opal is already salt-corrected or not) and so can the fluxes of any sedimentary component that is expected to be delivered vertically via particles, for example, biogenic barium.

3.3. Calculation of Errors and Systematic Uncertainties

In this section, two alternative approaches to determine the uncertainties resulting from error propagation are explored and compared. First, we present an analytical solution for the error propagation; second, we present a Monte Carlo simulation of the uncertainties.

3.3.1. Propagation of Analytical Errors in the Preliminary CRS age: Mathematical-Analytical Approach

A full error propagation of the analytical uncertainty for the final CRS age is demanding due to the iterative age determination, where the ingrowth of Th from authigenic U is calculated in the second step. However, we can test an analytical solution for error propagation of the first step, the preliminary CRS age, against the variability of the Monte Carlo simulation for the same step of the CRS model. The derivation of age uncertainties by propagation of errors in equation (13) involves the determination of the covariance of the two variables $I_{\geq i}$ and I. In order to avoid this, we rewrite equation (13) with independent variables following Appleby (2002):

$$t = -\frac{1}{\lambda_{230Th}}{}^{*}\ln\left(\frac{I_{\geq i}}{I_{<i} + I_{\geq i}}\right) \tag{21}$$

where $I_{\geq i}$ is the inventory above level i. Replacing A = $I_{\geq i}$ and B = $I_{<i}$

$$t = -\frac{1}{\lambda_{230Th}}{}^{*}\ln\left(\frac{A}{A+B}\right) \tag{22}$$

For uncorrelated A and B with standard deviations s_A and s_B, the error in t is given by:

$$s_t = \sqrt{\left(\frac{\partial t}{\partial A}\right)^2 {s_A}^2 + \left(\frac{\partial t}{\partial B}\right)^2 {s_B}^2} \tag{23}$$

$$s_t = \frac{1}{\lambda_{230Th}}\sqrt{\left(\frac{B}{A(A+B)}\right)^2 {s_A}^2 + \left(\frac{1}{A+B}\right)^2 {s_B}^2} \tag{24}$$

The resulting errors are shown in Figure 8.

3.3.2. Propagation of Analytical Errors in the Preliminary CRS age: Monte Carlo Approach

As an alternative approach to calculate the possible uncertainty in ages resulting from analytical uncertainties, we used a Monte Carlo approximation. This approach generates simulated data sets in

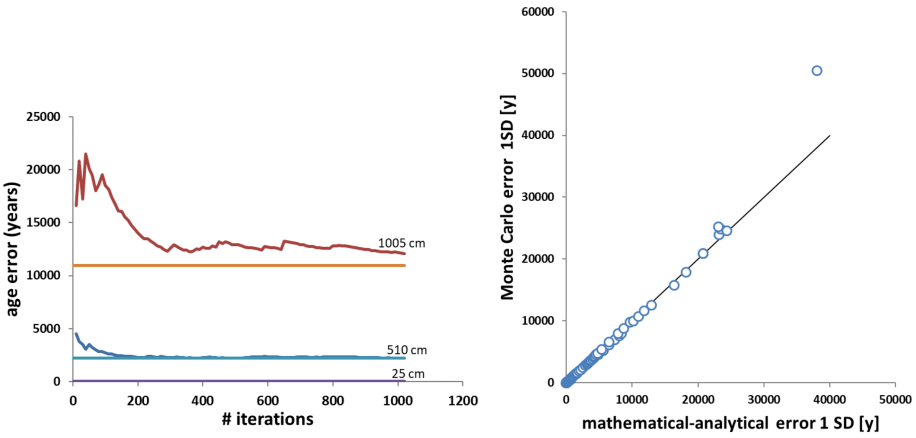

Figure 8. A comparison of the Monte Carlo error approximation and a mathematical-analytical solution estimating the uncertainties of the preliminary CRS age (no $^{230}Th_{auth}$ correction) from a propagation of analytical uncertainties. Left: The Monte Carlo error approaches a stable value as the number of iterations increases. Values from 25-, 510, and 1,005-cm depth have been chosen to show how the Monte Carlo uncertainty approaches the mathematical-analytical error (straight lines). The graphs would look different for each run of a Monte Carlo simulation. Right: Depth-by-depth comparison of the Monte Carlo simulation for n = 1000 and the mathematical-analytical solution, demonstrating agreement between the approaches for the preliminary CRS age.

which the actual analytical data are varied randomly as expected from their individual uncertainties. The CRS age is then calculated for a large number (here: n > 1000) of these simulated records, and the variation of the simulated age is used to derive the uncertainty that results from analytical errors. We allowed each of the values for $^{230}Th_{total}$, $^{232}Th_{total}$, and $^{238}U_{total}$ to vary as part of a normal distribution, using the analytical uncertainty to estimate the respective width of the distribution. Negative values for $^{230}Th_{ex}$ will occur as $^{230}Th_{ex}$ approaches zero with increasing age. These values were replaced by zero. This would have been done for the actual data as well. In addition, we allowed the factor for lithogenic ^{230}Th (0.48) to vary by 2% relative, as well as the actually measured WFD by 3% relative.

Our approach follows largely that of Sanchez-Cabeza et al. (2014). However, our determination of sample mass differed markedly because we only used discrete subsamples of about 75 mg instead of complete slices of a core. Therefore, we created a modified Monte Carlo model, which adds no depth uncertainty. The simulated raw data are propagated through the entire calculation, which allows an integrated assessment of uncertainties. At least 1000 iterations were performed to determine the variation of the model output. This is the value that we refer to when calculating the one sigma error. In addition, we recorded the respective maximum and minimum value of the Monte Carlo simulation in order to test the symmetrical distribution of the uncertainties.

3.3.3. Comparison of Mathematical-Analytical and Monte Carlo Approach

The comparison of the two approaches for estimating the uncertainty shown in Figure 8 demonstrates generally comparable errors. For old samples, the approximation of the error with the Monte Carlo approach might take more than 1000 iterations to reach a stable value, depending on individual simulation runs. However, the Monte Carlo approach has the advantage to be applicable for the estimation of the final CRS age as well, and it provides information on the symmetry of the error distribution, which would be implicitly assumed in a mathematical-analytical approach.

3.3.4. Propagation of Analytical Errors in the Final CRS age: Monte Carlo Approach

As the final CRS age is not an independent calculation from the preliminary CRS age, the underlying assumptions for a mathematical-analytical solution (independent variables, normal distribution) cannot be assumed to be valid. However, the Monte Carlo simulation, which has been shown to deliver a comparable error estimate for the preliminary CRS age (Figure 8), is not sensitive to these assumptions and can therefore be used to approximate the random uncertainties of the final CRS age as shown in Figure 5 (right).

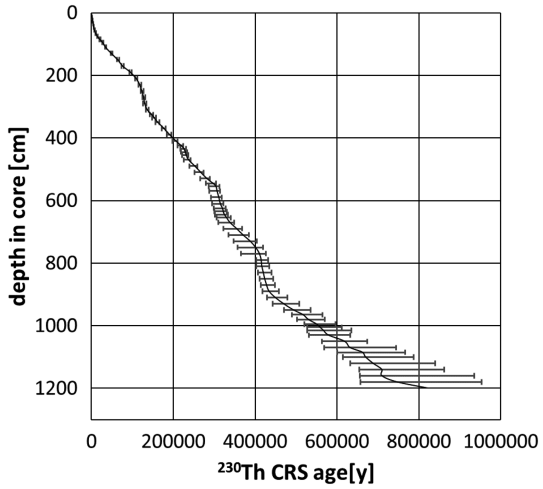

Figure 9. Depth versus $^{230}Th_{ex}$ CRS age, indicating the full range of Monte Carlo-simulated results as bars. This graph illustrates that analytical uncertainties result in a somewhat asymmetrical structure of age deviations. The older part of the record deviates more toward even older ages as a result of the logarithmic transformation in equation (2). The part above 800-cm deviates more toward younger ages as a result of an accidental high uncertainty in the ^{230}Th analysis of the 800-cm sample. CRS = Constant rate of supply.

3.3.5. Structure of Uncertainties: Are the Upper and Lower Uncertainties Symmetrical Throughout the Record?

The Monte Carlo approach allows a brief investigation of the symmetry of the age uncertainties. We used the simulated Monte Carlo records for PS63/146-2 to identify the extremes of the deviations. For each depth, we extracted the minimum and the maximum age of each depth of >1000 iterations. Figure 9 demonstrates that the obtained deviations due to analytical uncertainties are not fully symmetrical but depend on age and accidental changes in chemical-analytical uncertainty with depth. This implies that one should look not only at the normalized variance but also at the extremes of the distribution in order to understand the structure of uncertainties of the CRS model.

3.3.6. Systematic Uncertainties due to Focusing

3.3.6.1. Is the Supply of ^{230}Th Constant?

The CRS model does not require the ^{230}Th supply to be known; it only requires it to be constant through time. However, there are certain limits to this assumption, which we discuss in some detail below. Specifically, we address the role of variable focusing, which should be the main factor in causing deviations from a locally constant rate of supply.

It is well known that ^{230}Th flux varies through time due to focusing and winnowing—changes in sediment redistribution due to near-bottom water movements (François et al., 2004; Thomson et al., 1993). The degree of changes in focusing varies between sites. Values of full peak to trough ratios of three and above have been reported, but one should keep in mind that sampling is biased toward locations with focusing due to the demand for higher temporal resolution. For our site, we observe a focusing factor of 1.28:128% of the expected $^{230}Th_{ex}$ inventory found at the site.

In addition to focusing effects, a smaller variation in ^{230}Th supply could originate from changes in boundary scavenging. It has been shown that the combination of global ocean circulation and particle flux gradients leads to locally different ^{230}Th scavenging (Henderson et al., 1999). This in itself would not affect CRS dating with ^{230}Th, as long as it remains constant over time. However, this effect might also vary over time. We therefore decided to test the response of our ^{230}Th CRS-dating approach to such fluctuations in focusing and boundary scavenging in the following section.

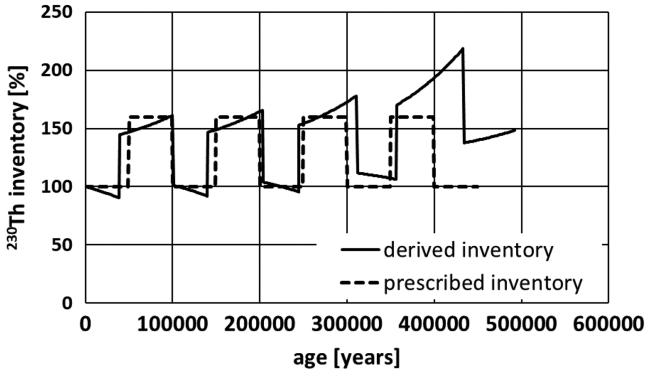

Figure 10. The prescribed initial ^{230}Th inventory versus prescribed (= actual) age of our simulated record (dashed line) and the derived initial ^{230}Th inventory versus the ^{230}Th CRS age (solid line). This graph visualizes that there is both an age offset as well as an offset in ^{230}Th inventories from the "real" ages and inventories. However, the offset is quantifiable and small compared to possible offsets from erroneous matching of stable isotope records. The deviation is smallest in the middle of the time interval, where the average focusing above and below is similar. CRS = Constant rate of supply.

3.3.6.2. Testing Sensitivity to Variations in ^{230}Th Supply by Alternating Focusing in a Simulated Core

In order to test the sensitivity of the dating approach to variations in ^{230}Th supply, we created an artificial record in which intervals of 50,000 years with a prescribed focusing factor of 1.6 ($\Psi = 1.6$) alternate with equally long intervals with no focusing ($\Psi = 1$). This results in an average focusing factor of 1.30, comparable to our actual record for PS63/146-2 with $\Psi = 1.28$ (128% of the produced ^{230}Th inventory). We then applied the decay equation to ^{230}Th in the artificial record and constructed the inventories that would be derived following equation (1) (assuming WFD = 1 and L = 1 and no U_{auth}). These inventories were used to calculate a CRS age according to equation (13). We then applied the decay correction from the derived CRS age to the artificial ^{230}Th record and use these decay-corrected data (artificial ^{230}Th with a realistic simulation of the CRS age correction) to calculate CRS-focusing factors (shown as % ^{230}Th inventory). We can then compare "prescribed inventory" versus "prescribed age" to "derived inventory" versus "derived age" (Figure 10).

We also determined the relative deviation of the CRS age from the prescribed age (Figure 11). We conclude that (a) for a variation in ^{230}Th supply of 60%, we obtain in general a realistic age distribution that would be

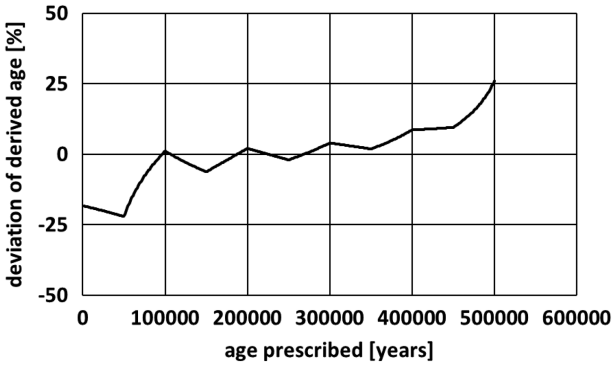

Figure 11. Deviation of the ^{230}Th CRS age from the prescribed age with alternating focusing and no focusing periods of 50,000 years ($\Psi = 1.6$ and $\Psi = 1$) in an artificial sediment record. CRS = Constant rate of supply.

sufficient for an initial decay correction. However, absolute dates are off by up to 25% in the earlier part of the records (b). Interestingly, the offset of the dating method is largest in the youngest and oldest parts of the record, whereas the middle of the record has the smallest deviations.

3.3.7. Uncertainties: How Do the Errors Compare to ^{210}Pb Dating?

The real uncertainties of the approach are difficult to assess from just theoretical considerations. Comparing it with ^{210}Pb CRS dating, for which decades of experience have been collected, ^{230}Th seems to be in a comfortable position. Some of the main issues of ^{210}Pb dating are much less problematic for ^{230}Th. Its analysis is faster and can be done more precisely due to the advantageous method (isotope dilution with sector-field inductively coupled plasma mass spectrometry vs. gamma counting or alpha counting), yet it requires more sophisticated equipment and sample processing. While not required for the application of a CRS model, the absolute production rate of ^{230}Th in seawater is much better constrained than that of ^{210}Pb from the atmosphere. We also are not aware of any instance where ^{230}Th has been found to be mobile in the dissolved phase in marine sediments, which may be another issue for some environments with ^{210}Pb. The key issue with ^{230}Th CRS dating, just like for ^{210}Pb$_{ex}$, is the requirement of a continuous, hiatus-free record and the effect of a possible variation in focusing, which we tried to assess in a first attempt with the simple model above. However, more records of ^{230}Th with independent age constraints will be needed to assess the limits of the concept.

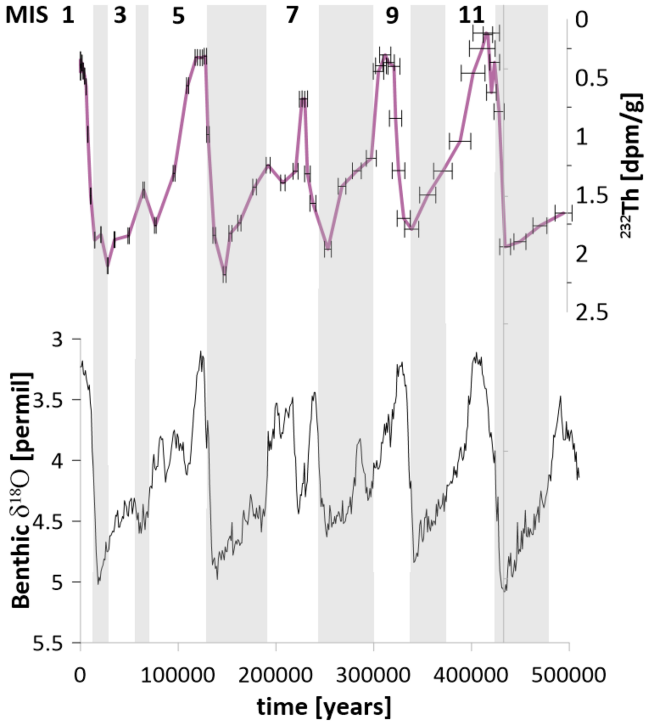

Figure 12. The content of ^{232}Th (indicator of the lithogenic fraction of sediments) versus ^{230}Th CRS age in the top panel and the benthic oxygen isotope stack according to Lisiecki and Raymo (2005) on its own age scale in the bottom panel. Glacial stages are shaded in grey for better comparability. Please note that both y axes are reversed. The record is cut off at 500,000 years to exclude ages beyond the range of the ^{230}Th$_{ex}$ CRS method. The similarity in timing between global oxygen isotope records and ^{232}Th concentration at this location is a clear indication that the ^{230}Th CRS-dating method delivers plausible age constraints. CRS = Constant rate of supply.

4. Results

In order to demonstrate the potential applications of a dated record with Th isotopes and elemental proxies available, we first compare the dated ^{232}Th signature to the global climate signal seen in oxygen isotopes of benthic foraminifera (Figure 12), and then we present the newly derived quantitative flux information from this core on an absolute age scale in comparison to a slightly more local dust signal (Figure 13).

4.1. Comparison of the Dated Record With the Oxygen Isotope Stack Record

4.2. Vertical Fluxes at the Core Location in Comparison With Dust Concentrations at EPICA Dome C (EDC) (Antarctica)

The method presented above permits the calculation of vertical fluxes of sedimentary components that are suitable for regional budgets, modeling studies or comparisons of sites in absolute units (Figure 13). For the site presented here as an example, we compare total mass fluxes, fluxes of biogenic silica, biogenic barium flux as a productivity proxy, and lithogenic fluxes to dust concentrations from EDC (Lambert et al., 2008) on their original age model. There are improved and slightly different age models for EDC data available (Bazin et al. (2013); maximum offsets in Figure 13 would be approximately 2 ky), but dust data would have required an interpolation of the original dust data set, while original published dates seem more convincing in this context. The data hint at an offset between peak lithogenic flux (presumably at the onset of the deglaciation) and peak productivity. Visual peak matching between lithogenic fluxes at PS63/146-2 and EDC dust concentrations hints at a certain age offset on the order of a few % for MIS7–MIS10, which is still within the uncertainty expected from propagation of analytical errors and deviations from constant flux discussed above.

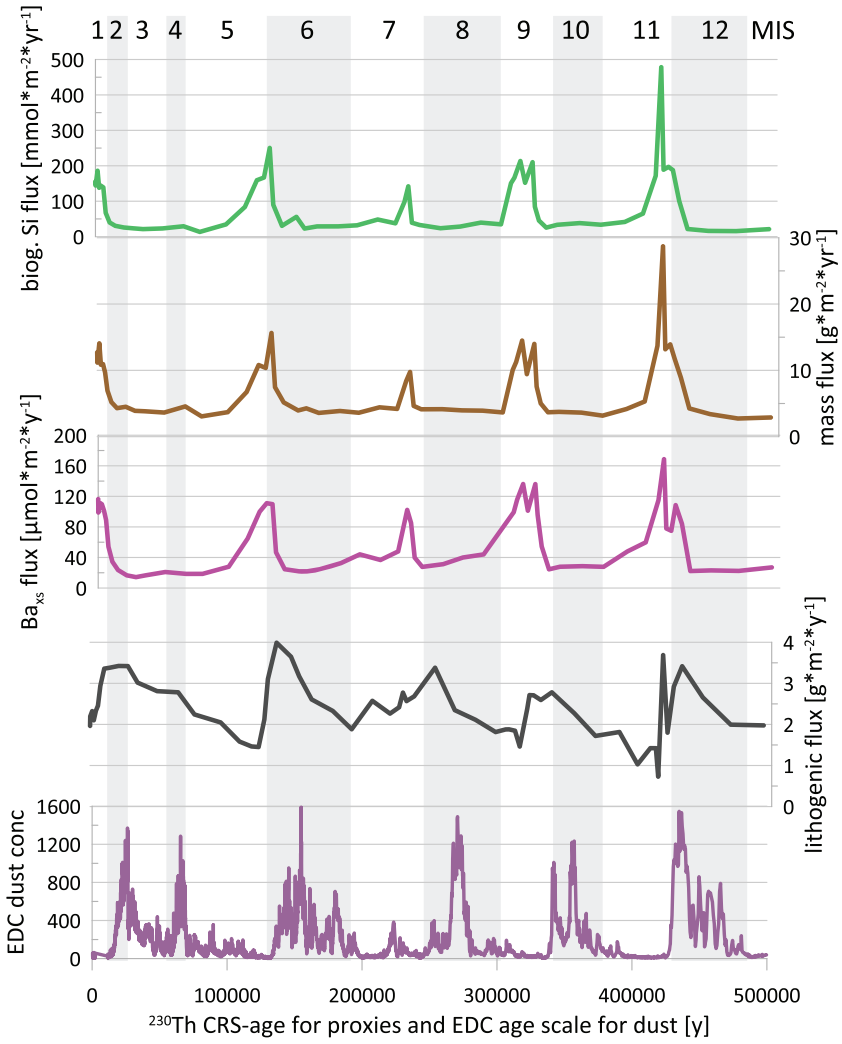

Figure 13. Preserved vertical fluxes of lithogenic material (estimated from ^{232}Th), biogenic opal, barium excess, and mass flux (salt free) versus ^{230}Th CRS age and EPICA Dome C dust concentrations on their independent age scales (see text) below. Biogenic fluxes are elevated at terminations and in interglacials, whereas lithogenic fluxes are steadily increasing from peak interglacials to the next termination, with some characteristic intermittent peaks. Dust concentrations from EPICA Dome C are shown for comparison (Lambert et al., 2008).

5. Discussion

5.1. Evaluation of the CRS-Dating Approach Under Variable Focusing Conditions at Sites With Existing Independent Age Information From Benthic Foraminiferal Oxygen Isotope Stratigraphy

In order to explore the suitability of the ^{230}Th CRS-dating approach at sites with known independent age constraints and established focusing conditions, we use the extensive ^{230}Th data set from Costa and McManus (2017) together with the stratigraphy from Costa et al. (2016). Three sites near the Juan de Fuca Ridge that display variable degrees of focusing (see Table 1) have been dated with the CRS approach, and the obtained dates were compared to the established stratigraphy (Figure 14). There is a small residual $^{230}Th_{ex}$ inventory missing that had to be estimated for applying the CRS approach because the cores were not analyzed to sufficient depths to reach background levels of ^{230}Th. This value is given in Table 1. For all cores, we report the observed inventory of ^{230}Th, the modeled residual inventory, and the expected inventory from production in the water column. The ratio of the total inventory to the expected inventory is an indicator of focusing, but it is strongly biased toward the young parts of the core that contribute the majority of the inventory.

Table 1
Characterization of the Three Sediment Cores From Costa and McManus (2017) With Respect to Focusing

Core	Range focusing factors (Ψ)	Observed $I^{230}Th$ [dpm/cm^2]	Modeled residual $I^{230}Th$ [dpm/cm^2]	Total $I^{230}Th$ [dpm/cm^2]	Expected $I^{230}Th$ [dpm/cm^2]	**Total $I^{230}Th$ vs. expected $I^{230}Th$**
39BB	0.4–1.7	818	23	841	811	**1.03**
35PC	0.8–3.4	1184	54	1238	793	**1.56**
09PC	0.5–2.9	1381	26	1407	778	**1.81**

Note. Residual ^{230}Th below the analyzed depths was modeled following a linear extrapolation of the logarithm of the activity of ^{230}Th.

The comparison demonstrates that for the core with the least pronounced focusing 39BB, dates agree well (Figure 14). A step in the ^{230}Th CRS age versus age curve at 272 ky is due to a disturbance that is observed in all three cores, introducing a deviation from a linear relationship. The symmetry of focusing conditions above and below a given depth is an important control on the fitness of the CRS model. If focusing is higher in the younger part, ages in the older part will be overestimated by the CRS model, which is what we observe to some extent for core 39BB. Core 35PC has more variable focusing conditions, in particular in the younger part, which creates relatively large deviations in this part of the core. For core 09PC, which is overall most affected by sediment redistribution, focusing is very asymmetrical between older and younger parts of the core and ages between the CRS model and the established stratigraphy deviate considerably and results in offsets of up to 50,000 years for the given ages around 200,000 years. Whether the accuracy of the CRS model or a specific focusing situation is sufficient for a given research question depends on the application. Our selection of deposition situations above tests a range of focusing conditions. We infer that the model delivers an excellent agreement for conditions with little or moderate variations in focusing intensity over time. Deviations from real ages become larger as the symmetry of focusing versus age diminishes.

Our Figure 14 also includes a curve for the age that would be obtained with an exponential fit of the ^{230}Th decay versus depth. This agreement is surprisingly good given the large amplitudes in mass flux of the cores that lead to quite variable $^{230}Th_{ex}$ activities. Still, it has the disadvantage that the fit will respond to both vertical mass flux and focusing, whereas the CRS model is not sensitive to changes in vertical mass flux. In fact, the difference in ages between various $^{230}Th_{ex}$ age models could be diagnostic for separating variations in mass flux from focusing.

5.2. Expected Limitations of the $^{230}Th_{ex}$ CRS-Dating Method

The potential accuracy and precision of the method is limited by the half-life of ^{230}Th but also by other physical factors. Bioturbation at the sediment surface homogenizes several cm of sediment, smoothing out signals and creating an offset in ages for low sedimentation environments. Shallow water depths lead to smaller $^{230}Th_{ex}$, increasing analytical uncertainties. Certainly a disadvantage is the requirement for a complete inventory of ^{230}Th. Experience from ^{210}Pb has shown that the CRS model responds quite sensitively to any residual inventory below the sampled depths in the older part of the record, which would make ages systematically too old. This can be countered with known independent age markers, if present, or an extrapolation of the missing inventory as used above for the set of Pacific cores. The uncertainty of such an estimate can be included in a Monte Carlo estimate of uncertainties. It should also be noted that $^{230}Th_{ex}$ is produced by a component of sea salt, leading to an implicit assumption of a constant inventory of salt overlying a core site. While this is a reasonable assumption for most deep sites, where increasing salinity in glacials is balanced by lower sea levels, shallower sites may experience less ^{230}Th input during periods of low sea levels. Sites underlying shelf ice, freshwater lenses, or a stream of icebergs will also receive less ^{230}Th, leading to a deviation from the basic CRS assumption under some extreme circumstances.

The $^{230}Th_{ex}$ CRS method can in principle be applied to historical ^{230}Th records, including data obtained by alpha spectrometry. However, very few such data sets have been published that cover the full $^{230}Th_{ex}$ inventory (i.e., going back >450,000 years) or at least a large part like the ^{230}Th records from Costa and McManus (2017) used above. In addition, sampling methods leave out a significant fraction of a core risk overlooking a part of the inventory. This limits the applicability to records of lower resolution and covering less than at least three ^{230}Th half-lives. The suitability of $^{230}Th_{ex}$ records covering only one or two glacial cycles for the CRS method needs to be judged carefully in view of the missing inventory and symmetrical focusing

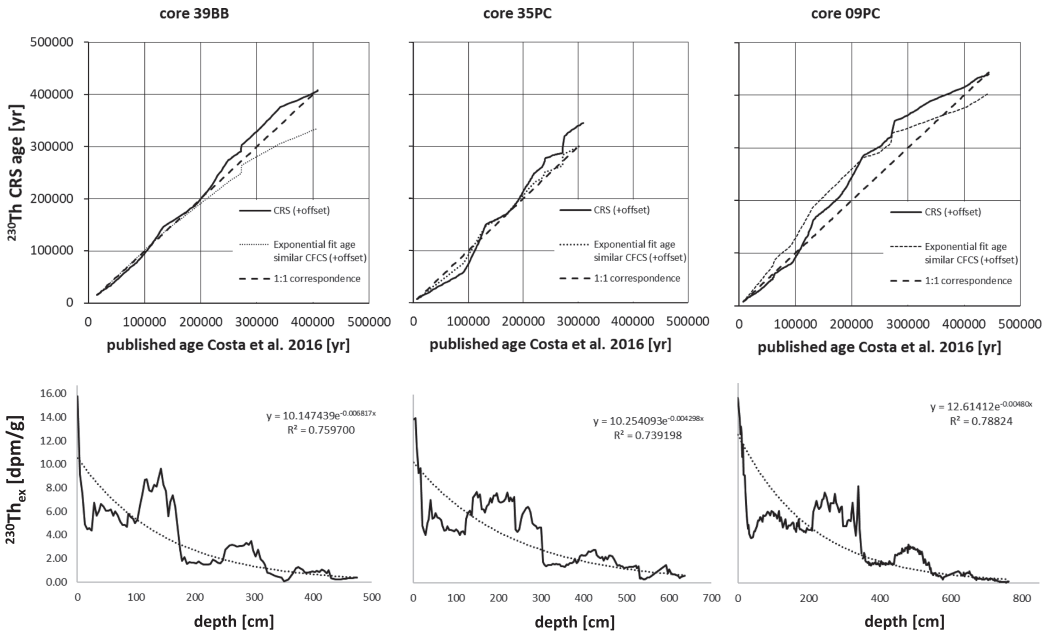

Figure 14. Comparison of the established stratigraphies with ^{230}Th CRS ages (dashed 1:1 line) and a simple exponential fit of ^{230}Th decay versus depth for three cores with variable focusing conditions (see Table 1). The bottom panel shows the respective activities of ^{230}Th$_{ex}$, which also respond strongly to variations in particle flux. CRS = Constant rate of supply.

throughout the record. For such short records, other independent age constraints are therefore needed. The analytical precision of historical records is less critical because the calculation of inventories reduces the impact of individual values on the CRS dates.

6. Conclusions

^{230}Th$_{ex}$ CRS dates have been found here to be a valuable addition to our dating toolbox for deep-sea sediments. They add absolute age constraints in an environment where most other dating approaches fail due to the absence of carbonaceous microfossils. We find that the age uncertainties due to analytical errors are below 10% if focusing intensity does not change strongly, and they can be well controlled. The main issue is certainly the possible age offset due to focusing. The possible extent of this offset can be estimated by comparing the full inventory of ^{230}Th in the entire core to the expected production and by an independent assessment of focusing variations in a part of the core with alternative dating methods. The method is not well suited to look at absolute dates in the youngest part of the record, but for ages of 50,000–450,000 years, deviations from true ages should usually be small, on the order of less than 10%.

For the new Southern Ocean record shown here, our absolute dating method has revealed a strong similarity between lithogenic contents, the global benthic oxygen isotope record, and dust deposition in Antarctica, which remains to be discussed in more detail elsewhere. This similarity can be used to this correlate this stratigraphy to neighboring cores and for matching marine paleorecords to ice core archives. While the applicability of ^{230}Th ends at approximately 500 ky, other radionuclides with a longer half-life, a sufficiently constant flux and a short oceanic residence time like ^{26}Al, could potentially extend the range of the CRS method to the entire Pleistocene.

Acknowledgments
We thank the principal scientist of cruise ANT XX/2, Prof. Dieter K. Fütterer, and the captain and crew of FS "Polarstern" for their support during and after the cruise. We thank Denise Bethke for her contribution to the analysis of the sediments. Kassandra Costa kindly provided the ^{230}Th data that allowed testing the robustness of our model against focusing. The data set is available at the Pangaea database (doi.pangaea.de/10.1594/PANGAEA.902257).

References

Anderson, R. F., Bacon, M. P., & Brewer, P. G. (1983). Removal of ^{230}Th and ^{231}Pa at ocean margins. *Earth and Planetary Science Letters*, *66*, 73–90. https://doi.org/10.1016/0012-821X(83)90127-9

Anderson, R. F., & Fleer, A. P. (1982). Determination of natural actinides and plutonium in marine particulate material. *Analytical Chemistry*, *54*(7), 1142–1147. https://doi.org/10.1021/ac00244a030

Appleby, P. G. (1998). *Dating recent sediments by 210 Pb: problems and solutions* (951-712-226-8, STUK-A145). Retrieved from Finland: http://inis.iaea.org/search/search.aspx?orig_q=RN:29040426

Appleby, P. G. (2002). Chronostratigraphic techniques in recent sediments. In *Tracking environmental change using lake sediments* (pp. 171–203). Dordrecht, Netherlands: Springer.

Appleby, P. G., & Oldfield, F. (1978). The calculation of lead-210 dates assuming a constant rate of supply of unsupported ^{210}Pb to the sediment. *Catena*, *5*(1), 1–8. https://doi.org/10.1016/S0341-8162(78)80002-2

Appleby, P. G., Oldfield, F., Thompson, R., Huttunen, P., & Tolonen, K. (1979). ^{210}Pb dating of annually laminated lake sediments from Finland. *Nature*, *280*, 53. https://doi.org/10.1038/280053a0

Bazin, L., Landais, A., Lemieux-Dudon, B., Kele, H. T. M., Veres, D., Parrenin, F., et al. (2013). An optimized multi-proxy, multi-site Antarctic ice and gas orbital chronology (AICC2012): 120–800 ka. *Climate of the Past*, *9*(4), 1715–1731. https://doi.org/10.5194/cp-9-1715-2013

Bollhöfer, A., Frank, N., Rohloff, S., Mangini, A., & Scholten, J. C. (1999). A record of changing redox conditions in the northern Peru Basin during the late Quaternary deduced from Mn/Fe and growth rate variations in two diagenetic manganese nodules. *Earth and Planetary Science Letters*, *170*(4), 403–415. https://doi.org/10.1016/S0012-821X(99)00126-0

Bourne, M. D., Thomas, A. L., Mac Niocaill, C., & Henderson, G. M. (2012). Improved determination of marine sedimentation rates using ^{230}Th$_{xs}$. *Geochemistry, Geophysics, Geosystems*, *13*, Q09017. https://doi.org/10.1029/2012GC004295

Costa, K. M., & McManus, J. (2017). Efficacy of ^{230}Th normalization in sediments from the Juan de Fuca Ridge, northeast Pacific Ocean. *Geochimica et Cosmochimica Acta*, *197*, 215–225. https://doi.org/10.1016/j.gca.2016.10.034

Costa, K. M., McManus, J. F., Boulahanis, B., Carbotte, S. M., Winckler, G., Huybers, P. J., & Langmuir, C. H. (2016). Sedimentation, stratigraphy and physical properties of sediment on the Juan de Fuca Ridge. *Marine Geology*, *380*, 163–173. https://doi.org/10.1016/j.margeo.2016.08.003

François, R., Frank, M., van der Loeff, M. M. R., & Bacon, M. P. (2004). Th-230 normalization: An essential tool for interpreting sedimentary fluxes during the late Quaternary. *Paleoceanography*, *19*, PA1018. https://doi.org/10.1029/2003PA000939

Frank, M., Eisenhauer, A., Bonn, W. J., Walter, P., Grobe, H., Kubik, P. W., et al. (1995). Sediment redistribution versus paleoproductivity change: Weddell Sea margin sediment stratigraphy and biogenic particle flux of the last 250,000 years deduced from Th-230(ex), Be-10 and biogenic barium profiles. *Earth and Planetary Science Letters*, *136*(3-4), 559–573. https://doi.org/10.1016/0012-821X(95)00161-5

Fütterer, D., & Kattner, G. (2005). Die Expedition ANTARKTIS-XX mit FS "Polarstern" 2002/2003: Bericht von den Fahrtabschnitten 1 und 2 = The expedition ANTARKTIS-XX of RV "Polarstern" in 2002/2003: reports of legs 1 and 2. *Berichte zur Polar-und Meeresforschung (Reports on Polar and Marine Research), 495*.

Geibert, W., Assmy, P., Bakker, D. C. E., Hanfland, C., Hoppema, M., Pichevin, L., et al. (2010). High productivity in an ice melting hotspot at the eastern boundary of the Weddell Gyre. *Global Biogeochemical Cycles*, *24*, GB3007. https://doi.org/10.1029/2009gb003657

Goldberg, E. D. (1963). Geochronology with ^{210}Pb. Paper presented at the symposium on radioactive dating (Athens, 19–23 Nov.1962). Proceedings Series of the International Atomic Energy Agency (STI/PUB/068).

Goldberg, E. D., & Koide, M. (1962). Geochronological studies of deep sea sediments by the ionium/thorium method. *Geochimica et Cosmochimica Acta*, *26*(3), 417–450. https://doi.org/10.1016/0016-7037(62)90112-6

Henderson, G. M., Heinze, C., Anderson, R. F., & Winguth, A. M. (1999). Global distribution of the ^{230}Th flux to ocean sediments constrained by GCM modelling. *Deep Sea Research Part I: Oceanographic Research Papers*, *46*(11), 1861–1893. https://doi.org/10.1016/S0967-0637(99)00030-8

Kominz, M. A., Heath, G. R., Ku, T. L., & Pisias, N. G. (1979). Brunhes time scales and the interpretation of climatic change. *Earth and Planetary Science Letters*, *45*(2), 394–410. https://doi.org/10.1016/0012-821X(79)90139-0

Ku, T. L. (1965). An evaluation of the U234/U238 method as a tool for dating pelagic sediments. *Journal of Geophysical Research*, *70*(14), 3457–3474. https://doi.org/10.1029/JZ070i014p03457

Ku, T.-L., & Broecker, W. S. (1965). Rates of sedimentation in the Arctic Ocean. *Progress in Oceanography*, *4*, 95–104. https://doi.org/10.1016/0079-6611(65)90043-1

Kuhn, G., Hillenbrand, C.-D., Kasten, S., Smith, J. A., Nitsche, F. O., Frederichs, T., et al. (2017). Evidence for a palaeo-subglacial lake on the Antarctic continental shelf. *Nature Communications*, *8*, 15591. https://doi.org/10.1038/ncomms15591

Lambert, F., Delmonte, B., Petit, J. R., Bigler, M., Kaufmann, P. R., Hutterli, M. A., et al. (2008). Dust-climate couplings over the past 800,000 years from the EPICA Dome C ice core. *Nature*, *452*(7187), 616–619. https://doi.org/10.1038/nature06763

Lisiecki, L. E., & Raymo, M. E. (2005). A Pliocene-Pleistocene stack of 57 globally distributed benthic delta O-18 records. *Paleoceanography*, *20*, PA1003. https://doi.org/10.1029/2004PA001071

Martínez-Garcia, A., Rosell-Melé, A., Geibert, W., Gaspari, V., Masqué, P., Gersonde, R., & Barbante, C. (2009). Links between Fe supply, ocean productivity, sea surface temperature and CO_2 over the last 1.1My. *Paleoceanography*, *24*, PA1207. https://doi.org/10.1029/2008PA001657

McGee, D., Marcantonio, F., & Lynch-Stieglitz, J. (2007). Deglacial changes in dust flux in the eastern equatorial Pacific. *Earth and Planetary Science Letters*, *257*(1), 215–230. https://doi.org/10.1016/j.epsl.2007.02.033

Niessen, F., Gebhardt, A., Kuhn, G., Magens, D., & Monien, D. (2013). Porosity and density of the AND-1B sediment core, McMurdo Sound region, Antarctica: Field consolidation enhanced by grounded ice. *Geosphere*, *9*(3), 489–509. https://doi.org/10.1130/GES00704.1

Pham, M., Sanchez-Cabeza, J., Povinec, P., Andor, K., Arnold, D., Benmansour, M., et al., & International Atomic Energy Agency (2008). A new certified reference material for radionuclides in Irish Sea sediment (IAEA-385). *Applied Radiation and Isotopes*, *66*(11), 1711–1717. https://doi.org/10.1016/j.apradiso.2007.10.020

Reimer, P. J., Bard, E., Bayliss, A., Beck, J. W., Blackwell, P. G., Ramsey, C. B., et al. (2016). IntCal13 and marine13 radiocarbon age calibration curves 0–50,000 years cal BP. *Radiocarbon*, *55*(4), 1869–1887. https://doi.org/10.2458/azu_js_rc.55.16947

Sanchez-Cabeza, J.-A., Ruiz-Fernández, A. C., Ontiveros-Cuadras, J. F., Pérez Bernal, L. H., & Olid, C. (2014). Monte Carlo uncertainty calculation of 210Pb chronologies and accumulation rates of sediments and peat bogs. *Quaternary Geochronology*, *23*, 80–93. https://doi.org/10.1016/j.quageo.2014.06.002

Sayles, F. L., Martin, W. R., Chase, Z., & Anderson, R. F. (2001). Benthic remineralization and burial of biogenic SiO_2, $CaCO_3$, organic carbon, and detrital material in the Southern Ocean along a transect at 170 West. *Deep-Sea Research Part II: Topical Studies in Oceanography*, *48*(19-20), 4323–4383. https://doi.org/10.1016/S0967-0645(01)00091-1

Taylor, S. R., & McLennan, S. M. (1995). The geochemical evolution of the continental crust. *Reviews of Geophysics*, *33*(2), 241–265. https://doi.org/10.1029/95RG00262

Thomson, J., Colley, S., Anderson, R., Cook, G. T., Mackenzie, A. B., & Harkness, D. D. (1993). Holocene sediment fluxes in the northeast Atlantic from Th-230(Excess) and radiocarbon measurements. *Paleoceanography*, *8*(5), 631–650. https://doi.org/10.1029/93PA01366

van Hulten, M., Dutay, J.-C., & Roy-Barman, M. (2018). A global scavenging and circulation ocean model of thorium-230 and protactinium-231 with improved particle dynamics (NEMO–ProThorP 0.1). *Geoscientific Model Development*, *11*(9), 3537–3556. https://doi.org/10.5194/gmd-11-3537-2018

Volz, J. B., Mogollón, J. M., Geibert, W., Arbizu, P. M., Koschinsky, A., & Kasten, S. (2018). Natural spatial variability of depositional conditions, biogeochemical processes and element fluxes in sediments of the eastern Clarion-Clipperton Zone, Pacific Ocean. *Deep Sea Research Part I: Oceanographic Research Papers*, *140*, 159–172. https://doi.org/10.1016/j.dsr.2018.08.006

Yang, H. S., Nozaki, Y., Sakai, H., & Masuda, A. (1986). The distribution of ^{230}Th and ^{231}Pa in the deep-sea surface sediments of the Pacific Ocean. *Geochimica et Cosmochimica Acta*, *50*, 81–89. https://doi.org/10.1016/0016-7037(86)90050-5

Erratum

The originally published version of Equation 7 contained errors introduced during the typesetting process. Equation 7 has been corrected, and this version may be considered the version of record.